Robust Increase in Supply by Vessel Dilation in Globally Coupled Microvasculature

Felix J. Meigel,[1] Peter Cha,[2] Michael P. Brenner,[2] and Karen Alim[1,3,*]

[1]*Max Planck Institute for Dynamics and Self-Organization, 37077 Göttingen, Germany*
[2]*John A. Paulson School of Engineering and Applied Sciences and Kavli Institute for Bionano Science and Technology, Harvard University, Cambridge, Massachusetts 02138, USA*
[3]*Physik-Department, Technische Universität München, 85748 Garching, Germany*

Neuronal activity induces changes in blood flow by locally dilating vessels in the brain microvasculature. How can the local dilation of a single vessel increase flow-based metabolite supply, given that flows are globally coupled within microvasculature? Solving the supply dynamics for rat brain microvasculature, we find one parameter regime to dominate physiologically. This regime allows for robust increase in supply independent of the position in the network, which we explain analytically. We show that local coupling of vessels promotes spatially correlated increased supply by dilation.

Vascular networks pervade all organs of animals and are the paradigm of adaptive transport networks. Their self-organized architecture continuously inspires the search for their underlying physical principles [1–4] and at the same time serves as a template for designing efficient networks in engineering [5]. The blood flowing through vessels transports nutrients, hormones, and metabolites to adjacent tissues. Metabolite exchange primarily occurs within the fine vessel meshwork formed by microvasculature. In the brain, local metabolite demand can abruptly rise due to an increase in neural activity [6], altering blood flow [7,8] in the same brain region, observable in fMRI [9]. During the process of increased neuronal activity, neurons signal their increased demand to adjacent astrocyte cells, which in turn trigger small ring muscles surrounding blood vessels to relax [10]. Thus, neural activity drives local dilation of a vessel [11,12], and hence regulates metabolite supply [7,13]. However, from a fluid dynamics perspective there is a mystery: blood vessels form a highly interconnected network in the microvasculature [8], resulting in a global coupling of blood flow. A single dilating vessel can potentially change the metabolite supply in a broad region of the network—and thus the local increase due to dilation is a function of specific network topology. Quantitatively, how much control over changes in blood-based supply resides in a single dilating vessel?

Models considering metabolite spread in tissue date back more than a hundred years to A. Krogh [14]. Krogh's model estimates the supply pattern in a tissue enclosed by vessels assuming that supply is constant on all vessel walls. Yet, on a larger tissue scale, supply spatially varies along the vasculature, since resources supplied upstream are not available downstream. Alternative models consider vessel-based transport [15], yet only diffusive transport is taken into account. The combined importance of advection

and diffusion for transporting solutes in a *single* tube was discovered by G. I. Taylor [16,17], with subsequent work outlining modifications due to solute absorption at the tube boundary [18–20]. Yet, there has been much less work capturing the coupling of advection and diffusion in tubular network structures [21,22], including solute absorption [23]. The impact of a dilating vessel is hard to estimate, since not only the absorption dynamics on the level of single vessels is changed, but also solute flux throughout the network is rerouted, since fluid flow and thus solute flux are globally coupled. However, to connect fMRI, which relies on a fluid dynamic signal [9,24,25], and the change in blood flow with neural activity [7,11,26–28], we need to understand how vessel dilations affect the supply with metabolites.

In this Letter, we present a theoretical model to determine the change in supply resulting from the dilation of a single vessel. On the level of an individual vessel, we analytically identify three regimes, each yielding a different functional dependence of the overall supply by absorption along the vessel wall on vessel geometry, blood flow, and blood-flow-based solute flux. Numerically analyzing supply dynamics in a microvasculature excerpt of a rat brain supplied from the Kleinfeld laboratory [8], we find that a single regime dominates. This regime has the important property that dilating a single vessel robustly increases the supply along the dilated vessel independent of the exact location of the vessel in the network. We explain analytically how a single vessel can buffer the global coupling of solute fluxes within the network and yield a robust local increase independent of network topology. We further discuss how a single dilating vessel impacts the solute flux downstream and thereby induces spatial correlations in supply increase.

To understand how a change in flow induces changes in solute flux and supply dynamics, we first focus on a single

228103-1

vessel. We assume that the flow is laminar with a longitudinal velocity profile $U(r) = 2\bar{U}[1 - (r/R)^2]$ [29,30], where $\bar{U}$ denotes the cross-sectional averaged longitudinal flow velocity. The dispersion of soluble molecules of concentration C by the fluid flow within a tubular vessel of radius R and length L is then given by

$$\frac{\partial C}{\partial t} + U(r)\frac{\partial C}{\partial z} = \kappa \nabla^2 C, \qquad (1)$$

where κ denotes the molecular diffusivity of the solute, and r and z parametrize the radial and longitudinal components of the vessel. The soluble molecule is absorbed at the vessel boundary, following

$$\kappa \frac{\partial C}{\partial r}\bigg|_{r=R} + \kappa \gamma C(R) = 0, \qquad (2)$$

with absorption parameter γ. In analogy to the derivation of *Taylor dispersion* [16,17,23], we simplify the multidimensional diffusion-advection for $C = \bar{C} + \tilde{C}$ to an equation for the cross-sectionally averaged concentration $\bar{C}$ if the cross-sectional variations of the concentration $\tilde{C}$ are much smaller than the averaged concentration itself. This is true if the timescale to diffuse radially within the vessel is much shorter than the timescale of advection along the vessel, $R^2/\kappa \ll L/\bar{U}$, if the vessel itself can be characterized as a long, slender vessel, $R \ll L$, and if the absorption parameter is small enough to keep a shallow gradient in concentration across the vessel's cross section $\gamma R \ll 1$, which states that the length scale of absorption is much bigger than the vessel radius. All these approximations are valid for the rat brain microvasculature example considered here [8]. With these assumptions, the concentration profile along the vessel approaches a steady state over a timescale $L/\bar{U}$ given by (see S1 in the Supplemental Material [31] for derivation)

$$\bar{C}(z) = C_0 \exp\left(-\beta(\text{Pe}, S, \alpha)\frac{z}{L}\right), \qquad (3)$$

$$\beta(\text{Pe}, S, \alpha) = \frac{24\text{Pe}}{48 + \frac{\alpha^2}{S^2}}\left(\sqrt{1 + \frac{8S}{\text{Pe}} + \frac{\alpha^2}{6\text{Pe}S}} - 1\right), \qquad (4)$$

where $\text{Pe} = \bar{U}L/\kappa$ is the Péclet number, $\alpha = \gamma L$, and $S = \kappa \gamma L/R\bar{U}$ measures the ratio of the absorption rate to the advection rate. Note that the concentration decays along the vessel starting from an initial concentration C_0 that itself is determined by the solute flux entering a vessel J_0. Also, for the solute influx into a vessel, the advective and diffusive transport contribute:

$$J_0 = \pi R^2 C_0 \left(\bar{U} + \frac{\kappa\beta}{L}\right) = \pi R^2 C_0 \bar{U}\left(1 + \frac{\beta}{\text{Pe}}\right). \qquad (5)$$

We define as the supply of a vessel ϕ the integrated diffusive flux through the entire vessel surface $\mathcal{S}$ of the cylindrical vessel,

$$\phi = -\int_{\mathcal{S}} \kappa \frac{\partial C}{\partial r}\bigg|_{r=R} 2\pi R \, dz. \qquad (6)$$

resulting in

$$\phi = J_0 \frac{1}{1 + \frac{\beta}{\text{Pe}}}\left(\frac{\frac{\alpha^2}{12S\text{Pe}} + 2\frac{S}{\beta}}{1 + \frac{\alpha^2}{4S\text{Pe}}}\right)[1 - \exp(-\beta)]. \qquad (7)$$

For physical intuition on how flow and vessel properties affect supply, we partition the phase space of supply dynamics spanned by Pe and S into three regimes, keeping α fixed; see Fig. 1. At large values of $S \gg 1$ and $S \gg 1/\text{Pe}$, the solute decays very quickly along the vessel. Here, all solute that flows into the vessel of cross-sectional area πR^2 is absorbed at the wall, here denoted the *all-absorbing regime*:

$$\phi_{\text{all}} \approx J_0 = \pi R^2 C_0 \bar{U}\left(1 + \frac{\beta}{\text{Pe}}\right). \qquad (8)$$

For a network, this implies that after a vessel in this regime, no solute for further absorption downstream of this vessel is available, which indeed is physiologically rare, 1.0% in the rat brain microvasculature considered here. A second regime occurs at $\text{Pe} \ll 1/S$, $\text{Pe} \ll S$, where diffusive transport dominates, here denoted the *diffusive regime*. We distinguish a third regime, which we denote the *advective regime*, where advective transport dominates,
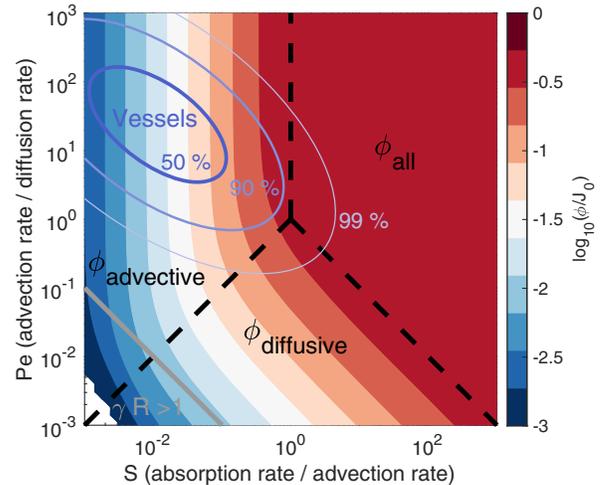

FIG. 1. Supply, ϕ, by a single vessel can be partitioned into three distinctive regimes as a function of dimensionless parameters characterizing flow and absorption, $\text{Pe} = \bar{U}L/\kappa$ and $S = \kappa \gamma L/R\bar{U}$. Dotted lines indicate separation of regimes. The remaining nondimensional parameter is fixed at $\alpha = 0.001$. Error ellipsoids contain the annotated percentage of vessels of the here-considered rat brain microvasculature [8] with physiological parameters for γ and κ; see the main text.

defined by $S \ll 1$ and $S \ll$ Pe. In both cases the solute decay is very shallow, $\beta \ll 1$ in Eqs. (3) and (7), resulting in supply independent of flow velocity, except for the dependence on the initial concentration C_0:

$$\phi_{\text{advective}} \approx \phi_{\text{diffusive}} \approx 2\pi RL\kappa\gamma C_0. \qquad (9)$$

Yet, note that the reason for the solute decay—i.e., β being small—arises from entirely different transport dynamics; see Fig. 1. This is reflected in the very different relations between initial solute concentration at the start of the vessel C_0 and the solute influx J_0 for the two regimes (see S1 in the Supplemental Material [31] for derivation):

$$J_{0,\text{advective}} \approx C_0\pi R^2\bar{U}, \qquad (10)$$

$$J_{0,\text{diffusive}} \approx C_0\pi R^{3/2}\kappa\sqrt{2\gamma}. \qquad (11)$$

Hence, under constant solute influx J_0, the diffusive and the advective regimes show fundamentally different, yet both nonlinear dependences on the vessel radius:

$$\phi_{\text{advective}} \approx J_0 \frac{2\gamma\kappa L}{R\bar{U}}, \qquad (12)$$

$$\phi_{\text{diffusive}} \approx J_0 \frac{\sqrt{2\gamma}L}{\sqrt{R}}. \qquad (13)$$

Based on these results for a single vessel, we expect largely varying increase in supply in response to vessel dilation. The coupling of flows and solute flux in a network is likely to make supply changes even more complex.

Within a network, not only are fluid flows coupled with every network node obeying Kirchhoff's law, $\sum_j \pi R_{\text{in},j}^2 U_{\text{in},j} = \sum_k \pi R_{\text{out},k}^2 U_{\text{out},k}$, but also solute flux J is conserved at every node, $\sum_j J_{\text{in},j} = \sum_k J_{0,k}$. Here, the solute influx $J_{\text{in},j}$ is determined by the inlet's vessel inflow $J_{0,j}$ upstream reduced by the amount of supply, ϕ_j, via that vessel; see Eq. (7). The influxes $J_{0,k}$ downstream a node, defined by Eq. (5), follow from the solute concentration at the network node C_0, given by

$$C_0 = \frac{\sum_j J_{\text{in},j}}{\sum_k \pi R_{\text{out},k}^2 (\bar{U}_{\text{out},k} + \kappa\beta_{\text{out},k}/L_{\text{out},k})}. \qquad (14)$$

Thus, solute fluxes are subsequently propagated from network inlets throughout the network.

To now investigate the impact of single-vessel dilation on supply within a network, we turn to an experimentally mapped rat brain microvasculature [8]. The data specify R, U, and L for all vessels, as well as the pressures at network inlets and outlets. Focusing on glucose as the primary demand, we account for glucose's diffusion constant $\kappa = 6 \times 10^{-10}$ m^2 s^{-1} [36] and estimate glucose's permeability rate, including $\gamma = 200$ m^{-1}; see S2 in the Supplemental Material [31]. Interestingly, we find 98% of all vessels to be

in the advective regime. Is there a functional property that makes the advective regime stand out?

We next quantify the change in supply due to vessel radius dilation in a capillary bed excerpt of the mapped rat brain microvasculature excluding pial and penetrating vessels. To this end, we use the pressures given in the dataset [8] and impose the pressure values at inlet and outlet vessels of a network excerpt. To be consistent with the flows determined within the dataset, we use a modified hydraulic vessel resistance to account for additional blood hematocrit resistance [37,38] in accordance with Blinder *et al.* [8]. Note that a vessel's hydraulic resistance is only important for calculating fluid flow velocities within vessels but does not modify the supply dynamics derived above. Pressures and hydraulic resistances then fully determine the flow velocities throughout the network due to Kirchhoff's law.

To identify differences in the behavior of the three supply regimes that may justify the physiological abundance of the advective regime, we sample the effect of vessel dilation for all three regimes, drawing randomly 120 vessels in each regime out of the total number of 21 793 vessels. The sheer total number of vessels allows us to sample the under-represented diffusive and all-absorbing regimes without introducing a statistical bias due to sample size. Each vessel's radius is dilated by 10%, and the flow and solute flux are recalculated throughout the network, keeping the network's inlet and outlet pressures fixed. The relative change in supply in the dilated vessel itself is evaluated in a histogram; see Fig. 2. Vessels in the all-absorbing regime
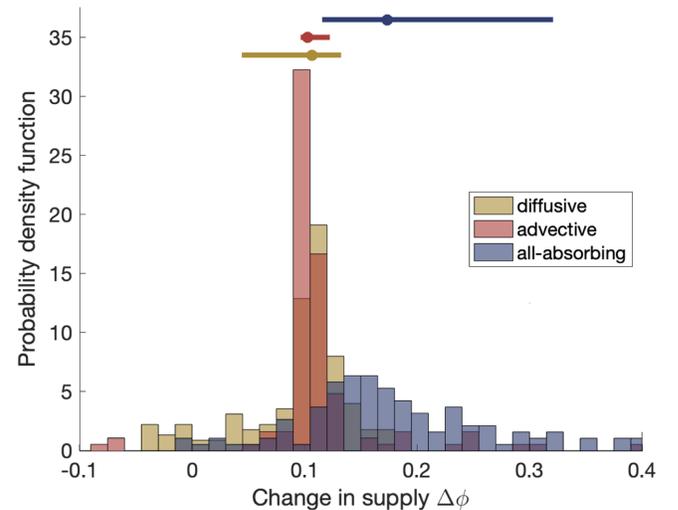

FIG. 2. The advective regime is robust in increasing supply by dilation. Histogram of change in supply $\Delta\phi$ due to a single vessel dilating by 10%. Lines indicate a range covering 69% with a percentage of 15.5% in both directions showing a lower or higher supply outside the indicated range. Big dots indicate the median, with values of 0.17, 0.10, and 0.11 for the all-absorbing, advective, and diffusive regimes, respectively. For each histogram, 120 vessels of the respective regime were randomly chosen and dilated.

show a broad response to vessel dilation. Vessels in the advective regime, in contrast, peak sharply at a robust 10% increase in supply, $\Delta\phi = 0.1$. The diffusive regime is also somewhat peaked around $\Delta\phi = 0.1$, but in addition shows a significant amount of vessels with a smaller supply increase of $\Delta\phi < 0.1$. Particularly, the advective regime shows a robust increase in supply, matching the increase in vessel diameter independent of the vessels' exact position within the network topology. This observation is robust against changes in the choice of the diffusion constant and permeability rate; see S6 in the Supplemental Material [31].

Despite our expectations of a nonlinear change in supply from single-vessel dynamics [Eqs. (12) and (13)], we find a robust increase of 10% for 10% vessel dilation, which would be reconciled within Eq. (9), if the initial concentration at the inlet of a dilating vessel C_0 [Eq. (14)] stays constant despite changes in flow and solute flux throughout the network. Which network properties allow C_0 to stay constant? What makes the advective regime more robust than the diffusive?

Let us consider a network node, where all vessels are in the advective regime with one inlet vessel and two outlet vessels, and where out of the latter, one is being dilated. Following Eq. (14) and the simplification of the solute fluxes from Eq. (10) for the advective regime, the initial concentration at the node is

$$C_0 \approx C_{\text{in}} \frac{\pi R_{\text{in}}^2 U_{\text{in}}}{\sum_k \pi R_{\text{out},k}^2 U_{\text{out},k}} = C_{\text{in}}, \qquad (15)$$

where Kirchhoff's law was used for further simplification. Hence, even though vessel radius dilation induces changes in the flow, $C_0 \approx C_{\text{in}}$ remains unchanged, though C_{in} might be affected by upstream changes in the supply. However, we find that upstream effects on C_{in} are small if the upstream vessels are in the advective or diffusive regimes—see S3 and S5 in the Supplemental Material [31]—which leaves C_{in} and thus C_0 approximately constant during vessel dilation. This result generalizes to good approximation to the case where the nondilating outlet vessel is in the diffusive rather than in the advective regime; see S3 in the Supplemental Material [31]. Note that the case where two inlet vessels merge into one outlet vessel is fundamentally different, as then the initial concentration at the node is a mixture from the two inlet vessels. Dilation of the outlet vessel changes flow in inlets differently and thereby changes the mixing ratio nonlinearly. Physiologically, we find this pattern especially closer toward venules. Taken together, these analytical results are in agreement with the statistics of Fig. 2 and explain in particular the robust increase in supply by dilation if the vessel is in the advective regime.

We next probe why the diffusive regime is less robust and revisit the setting of one inlet and one outlet in the advective regime, and the second outlet in the diffusive regime. But now, we compute the initial concentration at the node, given that we dilate the vessel in the diffusive regime:

$$C_0 \approx C_{\text{in,adv}} \frac{\pi R_{\text{in,adv}}^2 U_{\text{in,adv}}}{\pi R_{\text{out,adv}}^2 U_{\text{out,adv}} + \pi R_{\text{out,dif}}^{3/2} \kappa \sqrt{\gamma}}. \qquad (16)$$

Now the dilation of the vessel in the diffusive regime increases the denominator and thus leads to a decrease in the resulting C_0, rendering the diffusive vessel's response less robust compared to the advective. The same effect happens if all vessels at a node are in the diffusive regime, and even more so, as no vessel in the advective regime can buffer the dilation- and diffusion-dominated solute flux independent of flow velocity; see Eq. (11). Together, these analytical arguments explain why the diffusive regime yields a less robust increase in supply upon vessel dilation.

We found in Fig. 2 that the supply in an upstream vessel remains approximately constant during a single vessel dilation. What is the effect on vessels downstream of the dilated vessel? For this, we focus on the dilating vessel's immediate neighborhood and find that change in supply is spatially correlated (Fig. 3). We distinguish the vessels in the direct neighborhood of the dilated vessel in two categories: *downstream vessels* are vessels that are located directly downstream of the dilated vessel, and *parallel vessels* are vessels that are downstream of the node the dilated vessels branches from, but not downstream of the dilated vessel itself. The microvasculature dataset is known to show predominantly loop topologies, with a median size of eight vessels within a loop [8]. We thus considered only vessels with a topological distance of four vessels to the dilated vessel for the analysis of the immediate neighborhood. We find that the typical response of a dilating vessel in both the advective and diffusive regimes is to increase
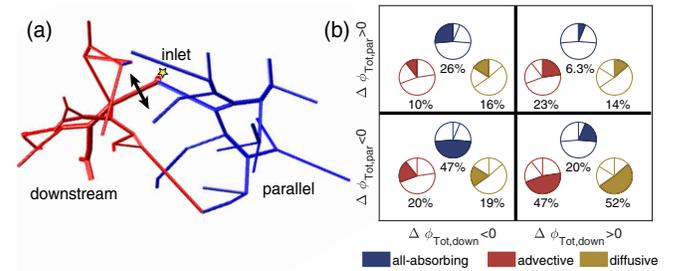
FIG. 3. The advective and diffusive regimes robustly increase supply downstream of a dilating vessel at the cost of decreasing supply in parallel vessels. (a) Enlargement of microvasculature excerpt exemplifying the neighborhood change in supply due to a single vessel dilation of 10% (advective regime, black arrow). Inlet marked by yellow star. Blue denotes a decrease, while red denotes an increase in supply in the individual vessels. The total change in supply is $\Delta\phi_{\text{tot}} = 6.4\%$ in the downstream vessels and $\phi_{\text{tot}} = 0.8\%$ in the parallel vessels. The change in C_0 for the dilating vessel is below $\Delta C_0 < 3 \times 10^{-4}$. (b) Neighborhood statistics of supply increase "+" or decrease "−" due to a dilating vessel in the respective regime. Evaluated is the overall change in supply in up to four vessels downstream or parallel to the dilated vessel chosen at the main inlet of a loop. The dilated vessel itself is excluded from the statistics here.

supply downstream at the cost of reducing supply in the parallel vessels [Fig. 3(b)]. More solute is drawn along the branch of the loop containing a dilating vessel than the dilating vessel itself is taking up, which increases the supply in downstream vessels. This is at the expense of the vessels in the parallel branch, reducing the supply there. See also S4 in the Supplemental Material [31]. While this applies qualitatively, the strength of this effect depends on the exact network topology.

We have provided a theoretical framework to investigate supply dynamics in a dynamically adapting tubular network, where flows are globally coupled by topology. We find that individual vessels can be classified into three regimes by vessel geometry and flow rate. Among these, particularly the regime governed by advective transport—and to a lesser extent, also the regime governed by diffusive transport—yields a robust increase in supply upon vessel dilation within the dilating vessel, notably leaving the supply pattern upstream unchanged and increasing supply immediately downstream. Interestingly, the most robust advective regime is found to dominate in brain microvasculature. Our findings therefore promote the idea that vessel dilation results in a robust increase in supply independent of the exact position of the vessel in the network. Our results are important for understanding the link between neural activity and patterns of change in supply invoked by vessel dilations and changes in blood flow underlying fMRI. Moreover, our framework is instrumental to predicting drug delivery and designing blood vessel architecture in synthetic organs, but it may also open entirely new avenues for the programming of soft robotics and smart materials.

[*] k.alim@tum.de

[1] C. D. Murray, Proc. Natl. Acad. Sci. U.S.A. **12,** 207 (1926).

[2] G. B. West, J. H. Brown, and B. J. Enquist, Science **276,** 122 (1997).

[3] D. Hu and D. Cai, Phys. Rev. Lett. **111,** 138701 (2013).

[4] H. Ronellenfitsch and E. Katifori, Phys. Rev. Lett. **117,** 138301 (2016).

[5] X. Zheng, G. Shen, C. Wang, D. Dunphy, T. Hasan, C. J. Brinker, Y. Li, and B.-L. Su, Nat. Commun. **8,** 14921 (2017).

[6] G. M. Boynton, S. A. Engel, G. H. Glover, and D. J. Heeger, J. Neurosci. **16,** 4207 (1996).

[7] M. E. Raichle and M. A. Mintun, Annu. Rev. Neurosci. **29,** 449 (2006).

[8] P. Blinder, P. S. Tsai, J. P. Kaufhold, P. M. Knutsen, H. Suhl, and D. Kleinfeld, Nat. Neurosci. **16,** 889 (2013).

[9] N. K. Logothetis, Nature (London) **453,** 869 (2008).

[10] B. A. MacVicar and E. A. Newman, Cold Spring Harbor Perspect. Biol. **7,** a020388 (2015).

[11] C. Cai, J. C. Fordsmann, S. H. Jensen, B. Gesslein, M. Lønstrup, B. O. Hald, S. A. Zambach, B. Brodin, and M. J. Lauritzen, Proc. Natl. Acad. Sci. U.S.A. **115,** E5796 (2018).

[12] R. A. Hill, L. Tong, P. Yuan, S. Murikinati, S. Gupta, and J. Grutzendler, Neuron **87,** 95 (2015).

[13] I. Vanzetta, R. Hildesheim, and A. Grinvald, J. Neurosci. **25,** 2233 (2005).

[14] A. Krogh, J. Physiol. **52,** 409 (1919).

[15] M. Schneider, J. Reichold, B. Weber, G. Székely, and S. Hirsch, Med. Image Anal. **16,** 1397 (2012).

[16] G. I. Taylor, Proc. R. Soc. A **219,** 186 (1953).

[17] R. Aris, Proc. R. Soc. A **235,** 67 (1956).

[18] E. M. Lungu and H. K. Moffatt, J. Eng. Math. **16,** 121 (1982).

[19] M. Shapiro and H. Brenner, Chem. Eng. Sci. **41,** 1417 (1986).

[20] G. N. Mercer and A. J. Roberts, Jpn. J. Ind. Appl. Math. **11,** 499 (1994).

[21] S. Marbach, K. Alim, N. Andrew, A. Pringle, and M. P. Brenner, Phys. Rev. Lett. **117,** 178103 (2016).

[22] Q. Fang, S. Sakadžić, L. Ruvinskaya, A. Devor, A. M. Dale, and D. A. Boas, Opt. Express **16,** 17530 (2008).

[23] F. J. Meigel and K. Alim, R. Soc. Interface **15,** 20180075 (2018).

[24] Y. He, M. Wang, X. Chen, R. Pohmann, J. R. Polimeni, K. Scheffler, B. R. Rosen, D. Kleinfeld, and X. Yu, Neuron **97,** 925 (2018).

[25] P. Tian, I. C. Teng, L. D. May, R. Kurz, K. Lu, M. Scadeng, E. M. C. Hillman, A. J. D. Crespigny, H. E. DArceuil, J. B. Mandeville, J. J. A. Marota, B. R. Rosen, T. T. Liu, D. A. Boas, R. B. Buxton, A. M. Dale, and A. Devor, Proc. Natl. Acad. Sci. U.S.A. **107,** 15246 (2010).

[26] O. B. Paulson, S. G. Hasselbalch, E. Rostrup, G. M. Knudsen, and D. Pelligrino, J. Cereb. Blood Flow Metab. **30,** 2 (2010).

[27] P. O'Herron, P. Y. Chhatbar, M. Levy, Z. Shen, A. E. Schramm, Z. Lu, and P. Kara, Nature (London) **534,** 378 (2016).

[28] C. M. Peppiatt, C. Howarth, P. Mobbs, and D. Attwell, Nature (London) **443,** 700 (2006).

[29] S.-S. Chang, S. Tu, K. I. Baek, A. Pietersen, Y.-H. Liu, V. M. Savage, S.-P. L. Hwang, T. K. Hsiai, and M. Roper, PLoS Comput. Biol. **13,** e1005892 (2017).

[30] D. Obrist, B. Weber, A. Buck, and P. Jenny, Phil. Trans. R. Soc. A **368,** 2897 (2010).

[31] See Supplemental Material at http://link.aps.org/supplemental/10.1103/PhysRevLett.123.228103 for further analytical derivation, parameter deduction, numerical routine and supporting figures, which includes Refs. [32–35].

[32] J. M. N. Duarte, F. D. Morgenthaler, H. Lei, C. Poitry-Yamate, and R. Gruetter, Front. Neuroenerg. **1,** 1 (2009).

[33] H. Fischer, R. Gottschlich, and A. Seelig, J. Membr. Biol. **165,** 201 (1998).

[34] W. L. Lee and A. Klip, Am. J. Physiol. Cell Physiol. **303,** C803 (2012).

[35] L. Leybaert, J. Cereb. Blood Flow Metab. **25,** 2 (2005).

[36] W. D. Stein, *Channels, Carriers, and Pumps: An Introduction to Membrane Transport* (Academic Press, New York, 2012).

[37] A. Pries, Cardiovasc. Res. **32,** 654 (1996).

[38] D. Rubenstein, W. Yin, and M. D. Frame, *Biofluid Mechanics*, An Introduction to Fluid Mechanics, Macrocirculation, and Microcirculation (Academic Press, New York, 2015).